JGR Space Physics

RESEARCH ARTICLE
10.1029/2022JA030798

Key Points:

- At higher altitudes the crests of Equatorial Ionization Anomaly (EIA) are found closer to the dip equator than the crests at lower altitude
- The positions of the EIA crests show a weak linear correlation with solar radio flux (F10.7)
- Empirical models for the position of EIA crests are developed

Correspondence to:

M. Nigussie,
melessewnigussie@yahoo.com

Citation:

Nigussie, M., Jakowski, N., & Hoque, M. (2022). Characterization and climatological modeling of Equatorial Ionization Anomaly (EIA) crest position. *Journal of Geophysical Research: Space Physics*, *127*, e2022JA030798. https://doi.org/10.1029/2022JA030798

Received 29 JUN 2022
Accepted 15 NOV 2022

Characterization and Climatological Modeling of Equatorial Ionization Anomaly (EIA) Crest Position

Melessew Nigussie[1], Norbert Jakowski[2], and Mainul Hoque[2]

[1]Washera Geospace and Radar Science Research Laboratory, Department of Physics, Science College, Bahir Dar University, Bahir Dar, Ethiopia, [2]German Aerospace Center, Institute for Solar-Terrestrial Physics, Neustrelitz, Germany

Abstract The Equatorial Ionization Anomaly (EIA) is characterized by strong ionospheric gradients that complicate ionospheric modeling and mitigation of ionospheric impact on Global Navigation Satellite System applications. In this study, the variation of EIA crest locations as a function of longitude and solar radio flux index F10.7 has been derived and modeled. Seven years (2013–2019) of ionospheric NmF2 and in-situ ion density data from Constellation Observing System for Meteorology Ionosphere and Climate and Swarm-A satellites have been used. We find that the distance between the northern and southern crest of EIA grows slightly with increase of solar flux. The position of the crests of EIA follows a wave number 4 structure with peak values at around −130°, 0°, and 100°E. At the altitude of Swarm-A (~460 km), the equatorial crests are found closer to the geomagnetic dip equator than they are at the peak density height hmF2 (~310 km) which may be due to the spatial variations of geomagnetic field strength. Accordingly, two Crest Position climatological Models have been developed, one for the F2 Peak height (CPM_F2P) and the other one for Swarm-A height (CPM_SAH).

1. Introduction

Solar Extreme Ultraviolet (EUV) and X-ray radiation are the main drivers for the formation of the ionosphere in the Earth's upper atmosphere. The variability of ionospheric ionization is described by changes in ionospheric parameters such as electron density or total electron content (TEC). The diurnal and seasonal variations of TEC, for example, are mainly due to diurnal and seasonal variations of solar radiation. As a result of the horizontal orientation of the geomagnetic field and eastward electric field, the equatorial low latitude ionosphere exhibits other unique ionospheric variations such as the Equatorial Ionization Anomaly (EIA) (e.g., Balan et al., 2018). EIA is characterized by the accumulation (EIA crest) and depletion (EIA trough) of ionized particles around ±15–20° magnetic latitude off and at the magnetic equator, respectively (Appleton, 1946; Balan et al., 2018; Huang & Cheng, 1996, 2013).

EIA is developed as a result of the competitive effect of diffusion, vertical $\mathbf{E} \times \mathbf{B}$ plasma drift, and neutral wind (Balan & Bailey, 1995). It shows different time scale variations including local time, day-to-day, season and solar cycle during quiet time periods (Huang, 1996; Huang et al., 2013). Using TEC data from the US Navy Navigation Satellite System, in the East-Asia sector, Huang and Cheng (1996) has shown that the strength of the EIA increases as the solar activity increases, but no significant solar cycle effect was observed in the occurrence time and latitude of the most developed EIA crest. Similarly, using International GNSS (Global Navigation Satellite System) Service (IGS) TEC from the Southeast-Asia sector, the strength, latitudinal, and occurrence time position of the EIA crest are found to be asymmetric with reference to the magnetic equator (Huang et al., 2013). The results from the Sheffield University Model showed that while the vertical $\mathbf{E} \times \mathbf{B}$ drift generates the plasma fountain and symmetric anomaly, the neutral wind introduces an asymmetry of the EIA (Balan et al., 2018; Balan & Bailey, 1995). The EIA crest positions are found to be around ±10° magnetic latitude due to the sole effect of diffusion; but when the vertical $\mathbf{E} \times \mathbf{B}$ drift and diffusion act together, the EIA crest positions can reach up to ±30° magnetic latitude (Balan et al., 2018). Moreover, Balan and Bailey (1995), computing electron density from a model driven by $\mathbf{E} \times \mathbf{B}$ drift and neutral wind speed, found that as the altitude increases the crest location was closer to the magnetic equator.

The presence of ionized particles in the Earth's ionosphere and their variations impact operation of GNSS applications such as navigation, positioning, and surveillance related to GNSS satellite communication (Arenas et al., 2016). GNSS applications are affected as a consequence of the delay of GNSS signal that is proportional

to the TEC or total loss of the signal due to radio scintillation effects (Arenas et al., 2016). The presence of EIA crests produces a strong gradient of TEC that aggravates the effect of TEC on the GNSS application (Arenas et al., 2016). While dual-frequency receivers minimize the effect of the ionosphere using differential techniques on L1 and L2 frequency measurements, the single frequency receiver is still vulnerable to the ionospheric impacts (Jakowski et al., 2011). The ionospheric effect on single-frequency GNSS receivers can be mitigated either by using an autonomous TEC empirical model or by using TEC observations from a GNSS signal monitoring network of dual frequency receivers (Arenas et al., 2016).

The well-known models for ionospheric error correction are Klobuchar, NeQuick 2, and Neustrelitz TEC Model (Neustrelitz TEC Model (NTCM)) (Jakowski et al., 2011; Klobuchar, 1987; Nava et al., 2008). The Klobuchar and NeQuick 2 models, respectively, are used for single-frequency error corrections for the Global Positioning System (GPS) and the European Galileo Satellite Navigation System (Galileo). These models are used to estimate the ionospheric delay by computing the ionospheric TEC along the GPS/GNSS signal raypath between the user and transmitter. The Klobuchar model has been designed, using a half cosine function and eight coefficients of two third-degree polynomials, to represent the diurnal, seasonal, geomagnetic latitude, longitude, and solar activity dependency of the delay (TEC) (JÚNIOR et al., 2019; Klobuchar, 1987). The nighttime delay (TEC) is represented by a constant delay that is 5 ns (9 TECu). The mathematical functions used in the NeQuick 2 are Epstein functions (electron density profiler). Ionospheric empirical models of peak parameters and slab-thickness are embedded together with the Epstein function (Nava et al., 2008). The NeQuick 2 provides TEC (or electron density) as a function of local time, season, geographic latitude and longitude, and solar activity. In NTCM, the product of five functions is being used to represent diurnal and semi-diurnal, annual and semi-annual, geomagnetic field, EIA crest, and solar activity variations of TEC (Jakowski et al., 2011). Fixed positions for northern and southern crests of the EIA such as 16° and −10°N magnetic latitudes, respectively, are used in NTCM. These fixed positions of crests of EIA imply that the crest positions are invariant of geographic longitude and also solar activity, even if studies indicated the dependence of the EIA crest on solar activity and other drivers such as diffusion, $\mathbf{E} \times \mathbf{B}$ drift, and neutral wind speed (Balan et al., 2018; Balan & Bailey, 1995) that have clear longitudinal and solar activity dependence. The studies presented above indicate none of the model include the effect of longitudinal variations of EIA; however, it is known that the existence of EIA complicates ionospheric modeling and mitigation of ionospheric effects due to strong ionospheric gradients that consequently produce problems in GNSS applications (Arenas et al., 2016; Jakowski & Hoque, 2019).

While it is important to study the EIA using models, like Balan and Bailey (1995), Huang et al. (2013) and Balan et al. (2018), it would be more complete and comprehensive to characterize the spatio-temporal variations of EIA using globally observed ionospheric parameters like in-situ electron density and NmF2. Therefore, in order to improve NTCM or to develop a new TEC empirical model, the variations of the positions of crests as a function of geographic longitude and solar flux should be characterized carefully, first and then modeled using ionospheric observations. In general, the purpose of this work is to answer the following research question: What latitude are the northern and southern crests of EIA located and does this position depend on solar activity? This question has been answered by characterizing ionospheric NmF2 and ion density observations from Constellation Observing System for Meteorology Ionosphere and Climate (COSMIC-1) and Swarm satellites, respectively. These satellite observations are very important because, unlike the ground GNSS receivers which are limited to land, COSMIC-1 and Swarm satellites provide excellent global coverage of observations, including above the oceans. Therefore, the main objective of this work is developing a climatological model of the location of the EIA crests to improve the climatological representation of the ionosphere for GNSS.

2. Data and Analysis Method

2.1. Data

This study of EIA location was conducted using data from two Low Earth Orbiting (LEO) satellites- Swarm A and COSMIC-1. Swarm constellation consists of three LEO satellites- A, B, and C. Their orbital plane is inclined at 87.35°. Satellites A and C rotate around the Earth at an altitude of 462 km side-by-side, separated by 1.4° longitude; satellite B rotates with the same inclination at an altitude of 511 km. These satellites are equipped with different onboard payloads such as the Electric Field Instrument that can measure the in-situ ion density. Swarm A 2 Hz sampling rate ion density observations, from 2014 to 2018, have been used for characterization and modeling purposes, whereas data from 2019 have been used for testing the model.

Similarly, COSMIC-1 mission was operational from 2006 to 2020. It flew over the Earth at an altitude of 800 km with an orbital inclination of 72°. GPS Radio Occultation (RO) TEC data from Cosmic-1 mission were used to estimate the electron density profile of the Earth's ionosphere and made available by University Corporation for Atmospheric Research for public use. Electron density profiles from 2014 to 2018 have been used for model development and analysis while data from 2013 have been used for model validation. NmF2 or hmF2, extracted from COSMIC-1 observations, found outside two-standard deviations were considered as outliers and not included in the analysis.

2.2. Analysis Methods

In this study, geomagnetically quiet time (Ap<15) data were used. NmF2 values have been extracted corresponding to quiet time electron density profiles obtained from COSMIC-1 all over the globe in the years 2013–2019. Each year, NmF2 values within 12–15 LT was averaged within a grid of 1° latitude by 8° geographic longitude. To remove small-scale oscillation of NmF2, a third order Butterworth low pass filter has been applied on the latitudinal variations of yearly average NmF2 obtained for each longitudinal sector. The smoothed NmF2 is convenient for identifying geographic latitude locations of the crests and troughs of EIA unambiguously. Similarly, in-situ ion density observations from Swarm A within 12–15 LT have been averaged over the same geographic grids. The same filtering technique was applied to smooth the geographic latitude variations of yearly average ion density.

From every 8° geographic longitude, 45 longitudinal sectors have been identified. For a clear visualization of EIA and identification of the geographic latitude position of crests and troughs, the map of yearly average NmF2 and ion-density have been developed. First, the maximum values of NmF2 and ion density from the geographic latitude variations of the yearly average NmF2 have been identified for each longitudinal sector and then the corresponding geographic latitudes of crests of EIA have been obtained. Similarly, the geographic latitude position of the trough of EIA has been identified corresponding to the minimum values of NmF2 and ion-density within the crest of the EIA.

The geographic latitudes of the crests and troughs of EIA, which have been identified corresponding to the maximum and minimum values of NmF2 and ion density, have been converted to magnetic latitudes (ϕ) using the International Geomagnetic Reference Field (IGRF) model available in the Python module and Equation 1

$$\phi = \tan^{-1}\left(\frac{1}{2}\tan(I)\right) \tag{1}$$

Where I is the geomagnetic inclination that can be obtained from the IGRF model driven by COSMIC-1 and Swarm observation parameters. The magnetic latitudes of the crests of EIA have been analyzed to investigate its variations with respect to (a) yearly average of daily 10.7 cm solar radio flux, and (b) geographic longitudes. The solar flux variations of the magnetic latitudes of crests have shown a linear relationship. Therefore, the linear model, which is given by Equation 2 has been used in the modeling process of the positions of the crests of EIA.

$$F_1 = a_o + a_1 F10.7 \tag{2}$$

Similarly, the geographic longitudinal (λ) variations of the magnetic latitude positions of crests, estimated for the 5 years, have been observed and sinusoidal functions have been proposed to capture this variation. The third harmonic cosine function (Equation 3) has been used for modeling the longitudinal variation of the position of the crests.

$$F_2 = A_o + A_1 \cos(\lambda + \varphi_1) + A_2 \cos(2\lambda + \varphi 2) + A_3 \cos(3\lambda + \varphi 3) \tag{3}$$

The product of Equations 2 and 3, that is, $F(\lambda, F10.7) = F1*F2$, has been fitted to the magnetic latitudes obtained from observations. Applying non-linear curve fitting techniques, using Python programming language, empirical models for magnetic latitudes for the northern and southern crests of EIA depending on geographic longitude and solar flux have been developed using data obtained in the years 2014–2018. The magnetic latitude model that has been developed using NmF2 data derived from COSMIC-1 is named as Crest Position Model (CPM) at F2 Peak (CPM_F2P); and similarly, the magnetic latitude model that has been developed using Swarm A ion density data is named as CPM at Swarm-A height (CPM_SAH). Therefore, CPM_F2P can be used to estimate magnetic

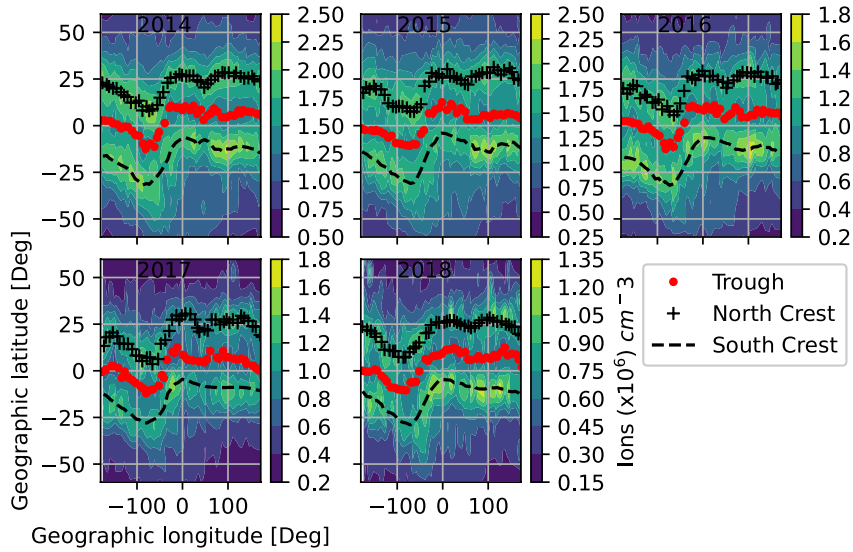

Figure 1. Geographic longitude and latitude variations of NmF2 obtained from RO electron density profiles of Constellation Observing System for Meteorology Ionosphere and Climate-1 satellite observations for the years 2014, 2015, 2016, 2017 and 2018; the geographic latitudes of the northern and southern crests and troughs are indicated respectively by line types "plus sign," "dashed," and "point marker".

latitudes of crests of EIA at the altitudes of NmF2 (~310 km), whereas CPM_SAH can be used to estimate the magnetic latitude of crests of EIA at the topside ionospheric (or at the altitudes of around 460 km). CPM_F2P and CPM_SAH models have been validated using observations in the years 2013 and 2019, respectively.

3. Results

3.1. Positions of EIA Crest and Trough

The in-situ ion density and NmF2 observations from Swarm A and Cosmic-1 satellites, respectively, have also been used to characterize the positions of the northern and southern crests of EIA. Figures 1 and 2 show the map of average NmF2 and ion density within 12 to 15 LT for every 1° geographic latitude by 8° geographic longitude

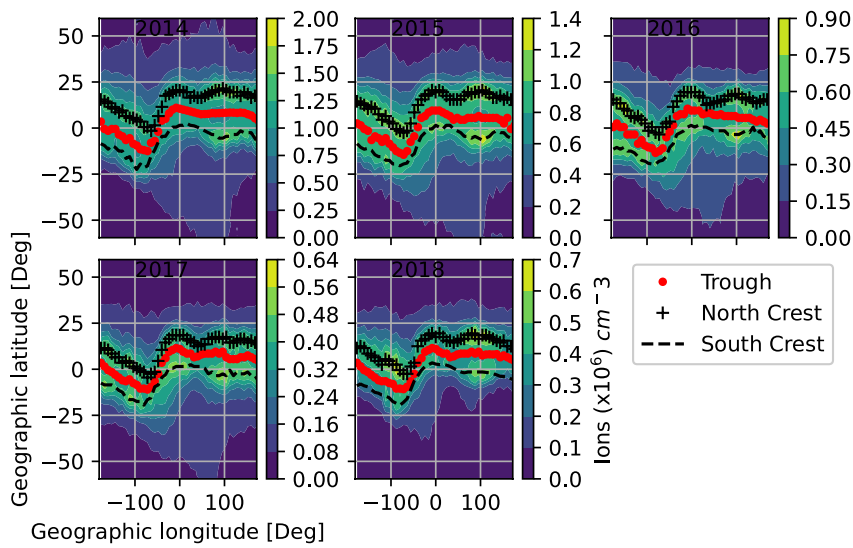

Figure 2. Geographic longitude and latitude variations of average ion density observed by Swarm A satellite years 2014, 2015, 2016, 2017 and 2018; the geographic latitudes of the northern and southern crests and troughs are indicated respectively by line types "plus sign," "dashed," and "point marker".

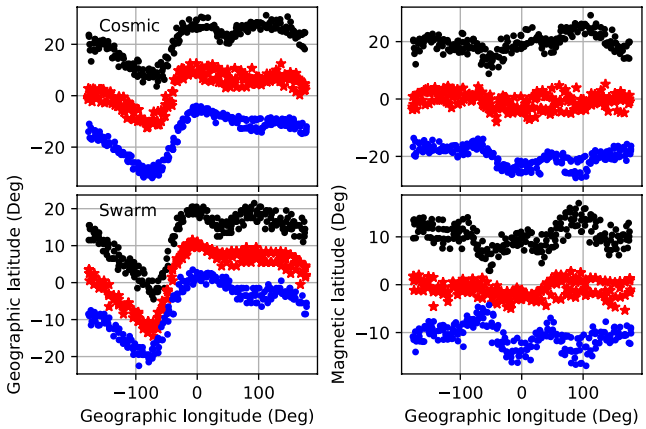

Figure 3. Geographic longitudinal variations of geographic (left panels) and magnetic (right panels) latitudes of crests and troughs of Equatorial Ionization Anomaly estimated from Constellation Observing System for Meteorology Ionosphere and Climate-1 NmF2 and Swarm A ion density observations for the years 2014, 2015, 2016, 2017, and 2018.

grid versus geographic longitude and latitude for the years 2014, 2015, 2016, 2017, and 2018. The geographic latitude locations of the northern and southern crests and troughs are marked in these figures. As seen in these figures, the longitudinal variation of the geographic latitude positions of the EIA crest and trough obtained from both satellites show a similar pattern. The Northern, Southern and Trough of EIA are denoted by line types of "plus sign," "dashed," and "point marker."

The geographic latitudinal positions of the crests and troughs shown in Figures 1 and 2 are extracted and displayed as a function of geographic longitude (see Figure 3). The left top and bottom panels of Figure 3 show the geographic latitudes of the crests and troughs obtained from COSMIC-1 NmF2 and Swarm A ion density observations, respectively for the years 2014–2018. The geographic latitude locations of the EIA crests and troughs from the data of both.

Satellites show similar geographic longitudinal variations. The corresponding magnetic latitude locations of the crests and troughs are shown in the right top and bottom panels of Figure 3. As seen, the magnetic latitudes of troughs estimated from both satellites concentrate around 0° magnetic latitude (see the red asterisks in the right panels of this figure). The geographic longitudinal variations of the magnetic latitudes for the northern and southern crests have shown sinusoidal patterns with three peaks around −130°, 0°, and 100°E geographic longitudes (which are also clearly visible in Figure 6). Around −50° and 100° geographic longitudes the magnetic latitude of the crests shows a maximum shift toward and away from the magnetic equator, respectively. Both the northern and southern crest magnetic latitude locations obtained from Swarm A are closer to the magnetic equator than the northern and southern crest locations estimated from Cosmic-1 NmF2 (see the right panel of Figures 3 and 6) and this result is in agreement with the findings of Balan and Bailey (1995). The average magnetic latitudes for the northern and southern crests estimated from the COSMIC-1 NmF2 are 19.7° and −20.1°, respectively. Similarly, the average magnetic latitudes estimated from Swarm A are 10.2° and −10.8°, respectively. These numbers clearly indicate that the Swarm ion density observation provides a position of crest closer to the magnetic equator compared to the corresponding crest positions estimated using COSMIC-1 NmF2 observations. The average magnetic latitude values obtained indicate that the Northern and Southern crest are positioned symmetrically with respect to the dip equator.

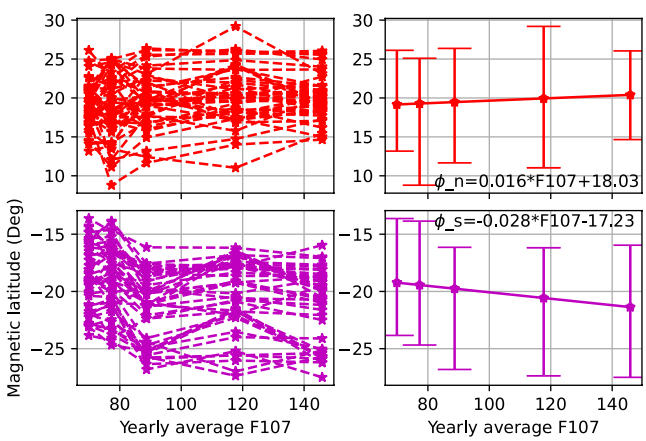

Figure 4. Magnetic latitudes of northern (top left) and southern (bottom left) crests versus yearly average F10.7 and their corresponding linear model output obtained using Constellation Observing System for Meteorology Ionosphere and Climate-1 NmF2 observations for the years 2014–2018.

3.2. EIA Crest Position Dependence on Solar Activity

Solar EUV, the main source of ionization of the ionosphere, has similar variations with the solar radiation at 10.7 cm (denoted by F10.7). As a result, the daily F10.7 is used as an indicator for solar activity variations. Yamazaki et al. (2010) have shown that the EEJ increases as F10.7 increases. The main driver for the EEJ is the zonal electric field at the E-layer ionosphere that can also influence the position of the EIA crests. Therefore, in this study the dependence of the position of EIA crests on F10.7 is examined. For this purpose, the yearly average magnetic latitude of EIA crests are estimated for different longitudinal sectors, have been plotted against the yearly average of daily F10.7 (see Figures 4 and 5). The yearly average values of F10.7 that are used for these plots are 69.9, 77.3, 88.7, 117.7, and 145.9 solar flux units (sfu) for the years 2018, 2017, 2016, 2015, and 2014, respectively. The left panels of Figures 4 and 5 show the magnetic latitudes for northern and southern crests, estimated from COSMIC-1 and Swarm A satellites observations, respectively versus yearly average F10.7. As seen from the left top and bottom panels of Figures 4 and 5, the position of the crests shifted away from the magnetic equator as the yearly average F10.7 increases. In general,

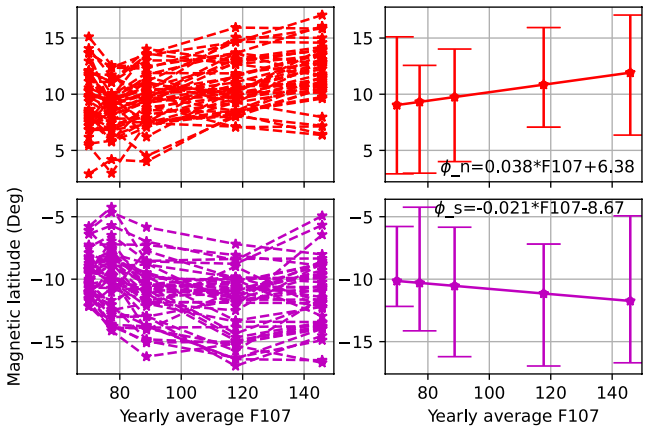

Figure 5. Magnetic latitudes of northern (top left) and southern (bottom left) crests versus yearly average F10.7 and their corresponding linear model output obtained using Swarm A ion density observations for the years 2014–2018.

the relationship between the magnetic latitudes and yearly average F10.7 looks linear and small which is consistent with the findings of Yamazaki et al. (2010).

As the linear relationship between solar flux and magnetic latitudes of EIA is evident from the left panel of Figures 4 and 5, a linear function has been used to fit to the 5 years of magnetic latitudes of the EIA crests. The linear model of the magnetic latitude of EIA crests is a function of yearly averaged solar flux that is presented in the right hand panels of Figures 4 and 5. The linear model for northern and southern crests are denoted by $\Phi_{\_n}$ and $\Phi_{\_s}$, respectively. The linear model obtained using NmF2 COSMIC-1 observations for the northern and southern crests, respectively are

$$\Phi\_n = 0.016 * F10.7 + 18.03 \quad (4)$$

and

$$\Phi\_s = -0.028 * F10.7 - 17.23. \quad (5)$$

Similarly, the linear models of the magnetic latitudes that have been developed from Swarm A observation are:

$$\Phi\_n = 0.038 * F10.7 + 6.38 \quad (6)$$

and

$$\Phi\_s = -0.021 * F10.7 - 8.67 \quad (7)$$

The rate of change of positions of magnetic latitudes of the northern crest, at the altitudes of the NmF2 (∼310 km) and around 460 km, are 0.016° and 0.038° magnetic latitude per F10.7, respectively. Similarly, the rate of change of positions of magnetic latitudes of crests of the southern hemisphere, corresponding to COSMIC-1 and Swarm A satellites, respectively are −0.028° magnetic latitude per F10.7 and −0.021° magnetic latitude per F10.7.

3.3. EIA Crest Position Modeling

Figures 4 and 5 present an obvious linear dependence of the EIA crest positions on magnetic latitude. The dotted lines (red color) in the left panel of Figure 6 depict the five years (2014–2018) of geographic longitudinal variations of average positions of magnetic latitude EIA crests obtained from COSMIC-1 and Swarm A satellites. The top two panels show the position of the crests of EIA for the Northern and Southern hemisphere obtained from the COSMIC-1 satellite, whereas the bottom two panels show the position of the crests obtained from the Swarm A satellite. As seen, the geographic longitudinal variations of the positions of EIA crests obtained from both satellites have shown a similar sinusoidal pattern. The sinusoidal patterns of the positions of the EIA crest with respect to longitude have shown three peaks at around −130°, 0°, and 100°E geographic longitudes. The linear and sinusoidal dependence of positions of the magnetic latitude on the solar flux and geographic longitude, respectively, have been captured by the product of third harmonics cosine (Equation 3) and linear (Equation 2) functions applying the non-linear curve fitting technique. The model parameters estimated through non-linear fitting, are provided in Table 1. The models corresponding to these satellites respectively are named as CPM_F2P and CPM_SAH.

The product of is the final model to estimate the position of EIA crests as a function of geographic longitude and solar radio flux. The output of these models as a function of F10.7 and geographic longitudes that have been used during curve fitting are over-plotted together with positions of EIA crests used for model development (see black asterisk lines in Figure 6). The right-hand panels of the same figure show the corresponding distribution of the differences of these model outputs and observations. As seen, the mismodeling distribution is nicely represented by Gaussian curves. The root-mean-square (rms), mean (μ) and standard deviation (σ) of the mismodeling are presented together with the distribution plots. The means of the mismodeling in all the cases are found to be about 0° whereas the standard deviations vary from 1.6 to 2.2°.

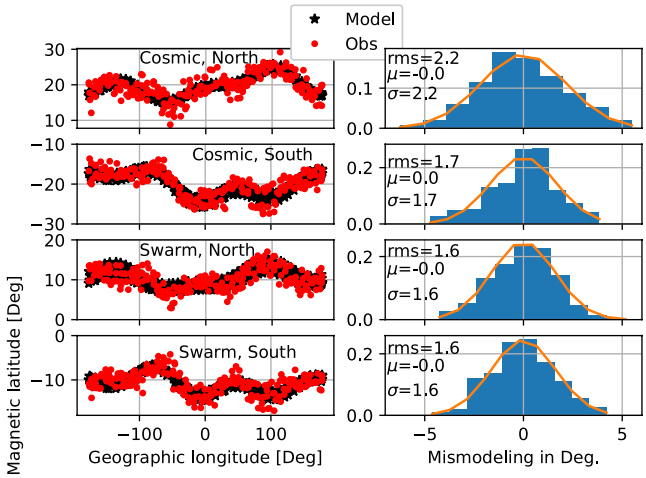

Figure 6. Geographic longitudinal variations of yearly average modeled (black asterisks) and observational (red dots) magnetic latitudes of Equatorial Ionization Anomaly crests (left panel) and the distribution of the mismodelings together with the Gaussian fit (right panel).

3.4. Model Validation of EIA Crests Positions

The performance of the CPM_F2P and CPM_SAH models are evaluated using observations obtained in 2013 from COSMIC-1 and in 2019 from Swarm A, respectively. The data from these years are used only for testing the performance of the models presented in Equations 2 and 3 together with the parameter values shown in Table 1. The top left and bottom panels of Figure 7 show the map of average NmF2 and ion density as a function of geographic latitude and longitude for the years 2013 and 2019, respectively. The geographic latitude positions of the northern (dash-dotted lines) and southern (dashed lines) crests of the EIA are over-plotted together with maps NmF2 and ion density, respectively. The corresponding modeled (solid lines) and observed (dashed lines) magnetic latitudes of the crests of EIA are also presented in the right-hand panels of the same figure. As seen, CPM_F2P and CPM_SAH modeled positions of the EIA crests show a nice agreement with the observations obtained between 12 and 15 LT.

The differences (or mismodeling) between observed and modeled positions of EIA crests shown in the right-hand panels of Figure 7 are computed and their distribution are presented in Figure 8. The top and bottom panels show the distribution of the mismodeling corresponding to CPM_F2P and CPM_SAH models, respectively. As seen in the top panels, the mean and standard deviations of mismodeling of CPM_F2P for both northern and southern crests are about 0 and 2°, respectively. Similarly, the standard deviation of the mismodelings corresponding to CPM_SAH for the northern and southern crests is about 1.5°. Also, the results not shown here indicate that the models perform well for post-sunset hours (between 18 and 21 LT).

4. Discussion

In the daytime, the E-layer dynamo dominating the F-layer dynamo generates the large-scale dawn-to-dusk electric field (E) (Farley et al., 1986). This electric field maps to the F-layer, almost without attenuation, and lifts the ionospheric plasma upward with $\mathbf{E} \times \mathbf{B}$ drift (Jin et al., 2008; Kil et al., 2007). When the vertically moving plasma loses momentum, it will slide along the geomagnetic field (B) line toward the north and south off the magnetic equator and ultimately produce the EIA. The left-hand side of Figure 9 shows the EIA crest positions, obtained from COSMIC-1 and Swarm A observations, versus longitude whereas the right-hand side shows the corresponding distances between north and south crests (in degree) and horizontal geomagnetic fields at the heights of 310 and 460 km versus geographic longitude. The geomagnetic field height (h) variations shown in the right-hand side is due to the general law that the geomagnetic field decreases with height. This geomagnetic field has also shown strong longitudinal variations. These geomagnetic field variations must have a significant effect on the strength of $\mathbf{E} \times \mathbf{B}$ upward drift, in other words, around 100°E the upward drift at the geomagnetic equator is significantly stronger than at around 60°W if we assume similar electric fields. A stronger uplift of the plasma automatically causes a wide spread of the plasma because higher L-shells reached by stronger uplifting having their ionospheric footprints at peak heights far away from the geomagnetic equator as observed and nicely seen in Figure 9. One can confirm this by observing the longitudinal variations of the distance between the north

Table 1
Estimated Model Parameter Values

Models	Model parameters									EIA crest
	A_o	A_1	A_2	A_3	φ_1	φ_2	φ_3	a_o	a_1	
CPM_F2P (from cosmic)	0.3972	−0.0553	−0.0315	0.0381	1.3523	0.5887	0.4018	45.5552	0.0394	North
	1.8238	−0.2975	0.0595	0.1490	−3.8579	0.7387	0.8119	−9.4701	−0.0153	South
CPM_SAH (from swarm)	1.2648	−0.2148	−0.172	0.134	0.7155	0.7816	1.1148	5.0585	0.0299	North
	1.736	−0.284	0.1067	0.2725	1.9361	−0.0842	0.7405	−4.9605	−0.0124	South

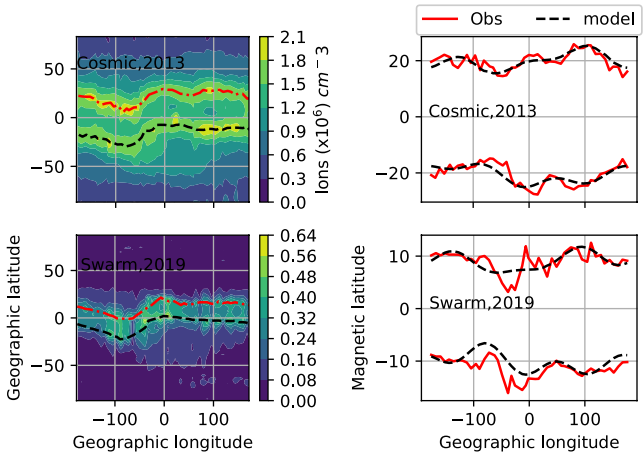

Figure 7. Geographic longitude and latitude variations of average NmF2 from Constellation Observing System for Meteorology Ionosphere and Climate-1 in the year 2013 and Swarm A in the year 2019 (left panels), modeled and observed magnetic latitude of northern and southern crests versus geographic longitude (right panels).

and south crest shown in the right-panel of Figure 9. The EIA plasma dynamics clearly indicates that the maximum of the uplifted plasma spreads down to lower altitudes along the field lines, that is, it is closer to the geomagnetic equator at greater heights, as seen from COSMIC-1 and Swarm observations in Figure 9. Similar to the results shown in Figure 9, Balan and Bailey (1995), using models, showed that as the altitude of observation increases, the EIA occurs at lower magnetic latitudes.

In addition, the positions of the EIA crests (see Figure 9) have shown a kind of periodic oscillations with varying amplitude as seen with respect to geographic longitude. The longitudinal oscillations of the EIA crest position is similar to the oscillation characteristics of the vertical **E** × **B** drift obtained from ROCSAT-1 observations within 1000–1100 LT in the years 1999–2004 (Kil et al., 2007). What is interesting about the similarity between the current and Kil et al. (2007) findings is that the oscillation peaks of the positions of EIA and vertical **E** × **B** drift velocity are found at similar geographic longitudes such as −130, 0, and 100°E. The conversion of the solar radiation energy to heat.

Induces the largest tides in the E-layer of the ionosphere (Forbes et al., 2003). The tidal wind in the E-layer through the ionospheric dynamo can modulate the large-scale electric field that ultimately produces the longitudinal variations of the zonal electric field that in turn produces a wave number 4 structure oscillation on the positions of EIA obtained in the current study, similar to a wave number 4 structure shown in different ionospheric parameters (Immel et al., 2006). It is also evident that the horizontal component of the geomagnetic field estimated just at the dip equator and fixed altitude decreases almost linearly from −180° to −66°E and from 98° to 180°E; on the other hand, it increases almost linearly as we go from −66° to 98°E. The smallest and largest magnitude of positions of the EIA, at a fixed altitude, respectively correlates with the smallest and largest values of the horizontal component of the geomagnetic field; this implies that the longitudinal variation of the geomagnetic field contributes to the longitudinal variations of the positions of EIA crests through the longitudinal variations of the vertical **E** × **B** drift. The other interesting feature observed is the symmetry of positions of the northern and southern hemisphere EIA crests. This symmetric character of the positions implies that the meridional wind that usually produces asymmetry in the EIA crest has been less dominant relative to the vertical **E** × **B** drift (Balan et al., 2018) that is expected to create symmetric characteristics of the EIA crests.

The E-layer ionization is due to the absorption of solar radiations such as X-ray and Extreme Ultraviolet (EUV). As it is not possible to measure the X-ray and EUV at the ground, before absorption by the atmosphere, the solar radio flux at 10.7 cm wavelength (denoted by F10.7) is being used as a good proxy for EUV ionizing radiation. Denardini et al. (2015), using radar observations, have shown low dependency of the zonal electric field on the F10.7. Similarly, Yamazaki et al. (2010) found that the linear dependence of the equatorial electrojet (EEJ) on F10.7 and the correlation between EEJ and F10.7 was 0.53. Yamazaki et al.'s (2010) result indicates a moderate correlation between the zonal electric field (driver of EEJ) and F10.7. In the current study, the rate of change of the positions of EIA for the northern and southern hemisphere are found to be from 0.016 to 0.038° magnetic latitude per F10.7 and from −0.028 to −0.021° magnetic latitude per F10.7, respectively. The rate of change of magnetic latitudes with a change of F10.7 found in the present work is small and the finding is similar to the findings of Yamazki et al. (2010) and Denardini et al. (2015).

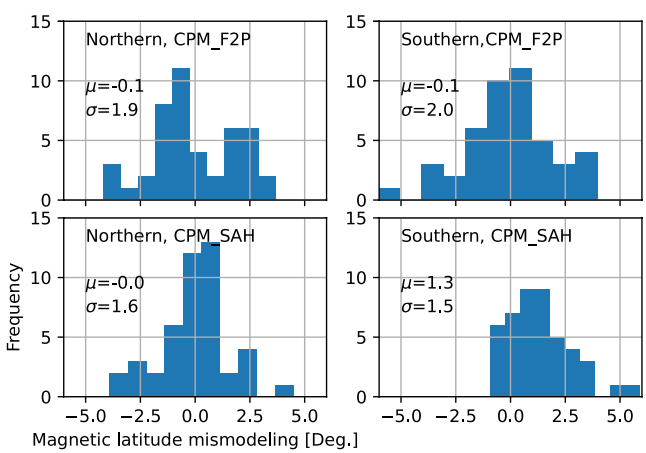

Figure 8. Distribution of the mismodeling residuals corresponding to CPM_F2P (top panels) and CPM_SAH (bottom panels) models for the years 2013 and 2019, respectively.

The modeling results obtained (Figures 6–8) have shown the basic longitudinal and solar flux variations of the position of EIA. For example, the smallest and largest modeled locations of EIA crests are obtained at the geographic locations where there are the lowest and highest extremes of geomagnetic field values. Also, the modeled positions of EIA crests have nicely shown the

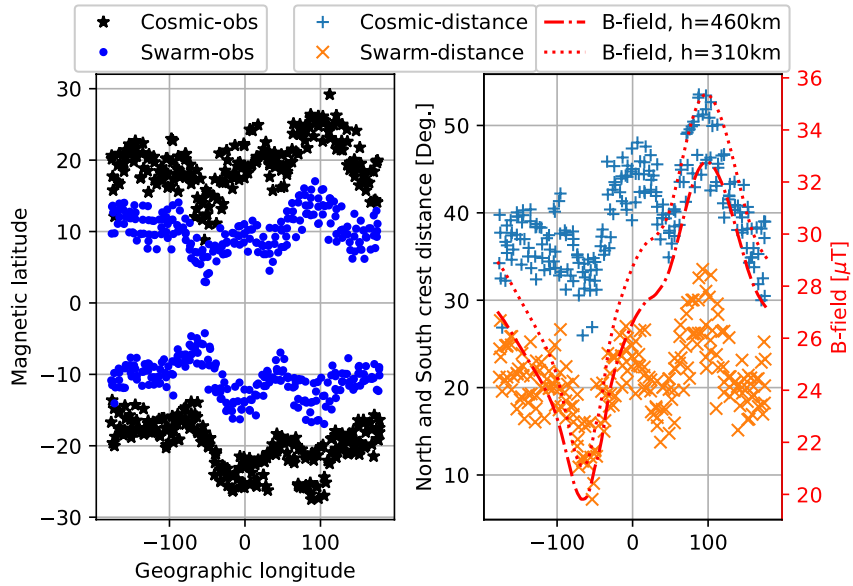

Figure 9. Observed magnetic latitudes of north and south Equatorial Ionization Anomaly crests corresponding to Constellation Observing System for Meteorology Ionosphere and Climate-1 and Swarm A satellites (left, denoted by asterisk and dotted lines) versus longitude; the distance between north and south crest position (in degree, denoted by +and x for COSMIC-1 and Swarm A respectively) and horizontal component of the geomagnetic field estimated from the International Geomagnetic Reference Field model at the heights of 310 km (dotted line) and 460 km (dash-dotted line), versus geographic longitude (right panel).

geographic longitudinal variations of observed positions of EIA. The CPM_F2P and CPM_SAH models, in estimating the northern and southern crests positions in the years 2013 and 2019, respectively, have shown about 2° and 1.5° standard deviations from the observed crest positions. These numbers indicate that the models developed are well representing both the northern and southern crest positions of the EIA.

5. Conclusions

The positions of the northern and southern crests of EIA have been estimated, analyzed, and modeled using Swarm A and COSMIC-1 observations in the years 2013–2019. The models developed are assumed to estimate the positions of northern and southern crests at the height of the peak electron density (~310 km) and at a 460 km height (orbital altitude of Swarm A) at any geographic longitude and yearly average solar flux. The performances of the models have been tested using data that have not been used for the model development (i.e., years 2013 and 2019). Based on the modeling and analysis work done in this study, the following conclusions are drawn:

- The positions of the crests of EIA depend on geographic longitude and solar activity. The relationship between the positions of crests of EIA and solar flux is found to be linear and the rate of change of the positions of crests of EIA per solar flux is found to be small (~0.016–0.038° magnetic latitude per F10.7 for the northern crest and about ~−0.028 to −0.021° magnetic latitude per F10.7 for the southern crest).
- The longitudinal variations of the positions of crests of EIA showed wave number 4 structure oscillations. Also, EIA crests at the higher altitude are found closer to the magnetic equator than the crests at the lower altitude and this is accounted for by the altitude variations of the horizontal component of the geomagnetic field over the dip equator.
- The models, which are developed in this study to capture the longitudinal and solar flux variations of the positions of the crests of EIA, are describing, with good accuracy, independently observed positions of crests of EIA (with the standard deviations varying from 1.5° to 2°).
- Therefore, based on the results obtained, it is recommended to embed the crest positions models of EIA developed in this study together with regional and global TEC models.

Data Availability Statement

The authors are also grateful to Swarm and COSMIC-1 mission teams for archiving ionospheric observations and making it available for public use: COSMIC-1 and Swarm data are accessed from: https://data.cosmic.ucar.edu/gnss-ro/cosmic1/postProc/level2/ and ftp://swarmdiss.eo.esa.int/Advanced/Plasma_Data/2_Hz_Langmuir_Probe_Extended_Dataset/, respectively. Moreover, the authors would like to thank the developers of Omniweb through which we access solar flux induces (https://omniweb.gsfc.nasa.gov/form/dx1.html) and the developers of the IGRF magnetic model written in Python that we have used to convert geographic latitudes to magnetic latitude.

Acknowledgments
The initial idea of this work has been supported by the DLR-DAAD research fellowship 2021 program. Also, the analysis and manuscript writing of this work have been supported by the Air Force Office of Scientific Research under award number FA8655-22-1-0001.

References

Appleton, E. V. (1946). Two anomalies in the ionosphere. *Nature*, *157*(3995), 691–693. https://doi.org/10.1038/157691a0

Arenas, J., Sardón, E., Sainz, A., Ochoa, B., & Magdaleno, S. (2016). Low-latitude ionospheric effects on SBAS. *Radio Science*, *51*(6), 603–618. https://doi.org/10.1002/2015RS005863

Balan, N., & Bailey, G. J. (1995). Equatorial plasma fountain and its effects: Possibility of an additional layer. *Journal of Geophysical Research*, *100*(A11), 21421–21432. https://doi.org/10.1029/95ja01555

Balan, N., Liu, L. B., & Le, H. J. (2018). A brief review of equatorial ionization anomaly and ionospheric irregularities. *Earth and Planetary Physics*, *2*(4), 257–275. https://doi.org/10.26464/epp2018025

Denardini, C. M., Moro, J., Resende, L. C. A., Chen, S. S., Schuch, N. J., & Costa, J. E. R. (2015). E region electric field dependence of the solar activity. *Journal of Geophysical Research: Space Physics*, *120*(10), 8934–8941. https://doi.org/10.1002/2015JA021714

Farley, D. T., Bonelli, E., Fejer, B. G., & Larsen, M. F. (1986). The prereversal enhancement of the zonal electric field in the equatorial ionosphere. *Journal of Geophysical Research*, *91*(A12), 13723–13728. https://doi.org/10.1029/ja091ia12p13723

Forbes, J. M., Zhang, X., Ward, W., & Talaat, E. (2003). Nonmigrating diurnal tides in the thermosphere. *Journal of Geophysical Research*, *108*(A1), 1033. https://doi.org/10.1029/2002JA009262

Huang, L., Huang, J., Wang, J., Jiang, Y., Deng, B., Zhao, K., & Lin, G. (2013). Analysis of the north–south asymmetry of the equatorial ionization anomaly around 110E longitude. *Journal of Atmospheric and Solar-Terrestrial Physics*, *102*, 354–361. https://doi.org/10.1016/j.jastp.2013.06.010

Huang, Y. N., & Cheng, K. (1996). Solar cycle variations of the equatorial ionospheric anomaly in total electron content in the Asian region. *Journal of Geophysical Research*, *101*(A11), 24513–24520. https://doi.org/10.1029/96ja01297

Immel, T. J., Sagawa, E., England, S. L., Henderson, S. B., Hagan, M. E., Mende, S. B., et al. (2006). Control of equatorial ionospheric morphology by atmospheric tides. *Geophysical Research Letters*, *33*(15), L15108. https://doi.org/10.1029/2006GL026161

Jakowski, N., & Hoque, M. M. (2019). Estimation of spatial gradients and temporal variations of the total electron content using ground-based GNSS measurements. *Space Weather*, *17*(2), 339–356. https://doi.org/10.1029/2018SW002119

Jakowski, N., Hoque, M. M., & Mayer, C. (2011). A new global TEC model for estimating transionospheric radio wave propagation errors. *Journal of Geodesy*, *85*(12), 965–974. https://doi.org/10.1007/s00190-011-0455-1

Jin, H., Miyoshi, Y., Fujiwara, H., & Shinagawa, H. (2008). Electrodynamics of the formation of ionospheric wave number 4 longitudinal structure. *Journal of Geophysical Research*, *113*(A9), A09307. https://doi.org/10.1029/2008JA013301

Júnior, S. P. T., Alves, D. B. M., & Silva, C. M. (2019). Klobuchar and nequick G ionospheric models comparison for multi-GNSS single-frequency code point positioning in the Brazilian region. *Bulletin of Geodetic Sciences*, *25*(3), e2019016. https://doi.org/10.1590/s1982-21702019000300016

Kil, H., Oh, S.-J., Kelley, M. C., Paxton, L. J., England, S. L., Talaat, E., et al. (2007). Longitudinal structure of the vertical ExB drift and ion density seen from ROCSAT-1. *Geophysical Research Letters*, *34*(14), L14110. https://doi.org/10.1029/2007GL030018

Klobuchar J (1987). Ionospheric time-delay algorithm for single frequency GPS users. In *IEEE transactions on aerospace and electronic systems, AES-23*. (pp. 325–332).

Nava, B., Cor¨sson, P., & Radicella, S. M. (2008). A new version of the NeQuick ionosphere electron density model. *Journal of Atmospheric and Solar-Terrestrial Physics*, *70*(15), 1856–1862. https://doi.org/10.1016/j.jastp.2008.01.015

Yamazaki, Y., Yumoto, K., Uozumi, T., Abe, S., Cardinal, M. G., McNamara, D., et al. (2010). Reexamination of the Sq-EEJ relationship based on extended magnetometer networks in the east Asian region. *Journal of Geophysical Research*, *115*(A9), A09319. https://doi.org/10.1029/2010JA015339